Kinetic energy dependence of dissociative charge–transfer reactions of He^+, Ne^+, Ar^+, Kr^+, and Xe^+ with silane

Ellen R. Fisher and P. B. Armentrout[a)]
Department of Chemistry, University of Utah, Salt Lake City, Utah 84112

(Received 19 April 1990; accepted 27 June 1990)

Guided ion-beam techniques are used to measure the cross sections as a function of kinetic energy for reaction of SiH_4 with He^+, Ne^+, Ar^+, Kr^+, and Xe^+. State-specific data for the $^2P_{3/2}$ ground spin–orbit states of Kr^+ and Xe^+ are also obtained. The products observed in the He, Ar, and Kr systems are SiH_x^+ for $x=0$–3. For the Ne system, formation of SiH_x^+ $x = 0$–2, is seen, while in the Xe system only SiH_3^+ and SiH_2^+ are observed. Reactions of He^+, Ne^+, Kr^+, and Xe^+ show little dependence on kinetic energy, but for the case of Ar^+, the reaction probability and the product distribution are highly sensitive to the kinetic energy of the system. Thermal reaction rates for all of the reactions are derived and compared with previous measurements. The results for these reactions are explained in terms of vertical ionization from the $1t_2$ and $3a_1$ bands of SiH_4. The relationships of these reactions to plasma deposition and etching are also discussed.

INTRODUCTION

In the last few years, deposition techniques using plasmas have been widely used in the fabrication of microelectronic devices.[1] Hydrogenated amorphous silicon films (α-Si:H) prepared by plasma decomposition of silane are of interest as potential solar photovoltaic energy convertors[2] and xerographic photoreceptors.[3] Reactors for the production of these films typically have reagent gas compositions of up to 50% silane. The remaining components include rare gas buffers, such as helium or argon, and sometimes molecular hydrogen. The amount and type of rare gas diluent has been seen to significantly alter the deposition characteristics for silane.[4] Specifically, films produced with He and Ne as the diluent gas have markedly different film properties and deposition rates than films where Ar and Kr are present. These differences are proposed to be due to an increase in the SiH_x^+ ($x = 1$–3) ion density in the Ne/SiH_4 and He/SiH_4 plasmas caused by reactions with metastable states of the rare gases.[4]

Reactions between rare gas ions and silane have been studied previously via ion cyclotron resonance (ICR)[5,6] and drift tube techniques.[7] Using ICR methods, Bowers and Elleman (BE) report thermal energy rate constants for Xe^+, Kr^+, Ar^+, Ne^+, and He^+ with SiH_4 and discuss their results in relation to Franck–Condon factors. Chatham *et al.* report rate constants and product ion distributions from their drift tube experiments for the reactions of Ar^+, Ne^+, and He^+ with silane over a narrow energy range of 0.1–1.0 eV.[7] These results are in reasonably good agreement with those of BE for the Ne and He systems, but do not agree in the case of Ar. The most recent study of reaction rates for these systems is included in a Fourier transform ICR study of the kinetics of silane plasmas.[6] There is again some discrepancy between these values and those of previous studies.

Recent work in our laboratory has focused on ion–molecule reactions related to plasma systems involving CF_4,[8] SiF_4,[9,10] $SiCl_4$,[11] and SiH_4.[12,13] Two of these studies focus on the reactions of rare gas ions with SiF_4[10] and CF_4.[8] The present work is a continuation of these studies, and was undertaken for several reasons. First, we wish to measure the effect of kinetic energy on these reactions. Such information is important to a detailed understanding of plasma deposition processes since plasma systems contain ions with a wide range of kinetic energies. Second, we wish to understand the interaction between kinetic energy and Franck–Condon factors for such dissociative change–transfer reactions. A similar analysis was made in the study of the reactions of Ar^+, Ne^+, and He^+ with CF_4,[8] and a strong coupling between translational and electronic energy was found. Finally, we want to help resolve discrepancies between the various literature reaction rates at thermal energies, while also providing rate constants over a wide range of kinetic energies. These data are important to computer modeling of plasma chemistry since thermal rate constants need not be applicable to the energies in the entire plasma environment.[14]

EXPERIMENTAL SECTION

General

The ion beam apparatus and experimental techniques used in this work are described in detail elsewhere.[15] The rare gas ions are produced as described below. The $^4He^+$, $^{22}Ne^+$, $^{40}Ar^+$, $^{84}Kr^+$, and $^{132}Xe^+$ ions are each mass analyzed and decelerated to the desired translational energy. The $^{22}Ne^+$ isotope was used due to contamination by an impurity ion of mass 20 in the $^{20}Ne^+$ beam. The ion beam is injected into an rf octopole ion beam guide,[16] which passes through the reaction cell containing the neutral reactant gas. The neutral pressure is sufficiently low, 0.01 to 0.07 mTorr, that multiple ion–molecule collisions

[a)]Camille and Henry Dreyfus Teacher–Scholar, 1987–1992.

 0021-9606/90/194858-10$03.00

are improbable. The unreacted rare gas and product ions drift out of the gas chamber to the end of the octopole, where they are extracted and analyzed in a quadrupole mass filter. Ions are detected by a secondary electron scintillation ion counter using standard pulse counting techniques. Raw ion intensities are converted to absolute reaction cross sections as described previously.[15]

Laboratory ion energies (lab) are converted to energies in the center-of-mass frame (C.M.) by using the conversion $E(\text{C.M.}) = E(\text{lab}) \cdot M/(m+M)$, where m is the ion mass and M is the neutral molecule mass. Unless stated otherwise, all energies quoted in this work correspond to the C.M. frame. The full-width at half-maximum (FWHM) of the ion kinetic energy distribution is determined by using the octopole beam guide as a retarding potential analyzer.[15] The uncertainty in the absolute energy scale is ± 0.05 eV (lab). The distribution of ion energies has an average FWHM of 0.6 eV (lab) for He^+, 0.4 eV (lab) for Ne^+, and 0.3 eV (lab) for Ar^+, Kr^+, and Xe^+.

Ion source

The rare gas ions are produced by electron impact (EI) of helium, neon, argon, krypton, or xenon gas, which have ionization energies (IE) of 24.580, 21.559, 15.755, 13.9997, and 12.130 eV, respectively.[17] The first excited electronic states of the ions are 65.4, 48.5, 29.3, 27.5, and 23.4 eV, respectively, above the neutral ground states.[17] Since the electron energy is variable, it can easily be kept below the threshold for formation of ionic excited states. The nominal electron energies used are thus 60 eV for He^+, 40 eV for Ne^+, 25 eV for Ar^+, 23 eV for Kr^+, and 20 eV for Xe^+. Only the $^2S_{1/2}$ ground state of He^+ is formed, but both the $^2P_{3/2}$ and $^2P_{1/2}$ spin–orbit states of the other rare gas ions are produced. The $^2P_{1/2}$ states of Ne^+, Ar^+, Kr^+, and Xe^+ lie 0.097, 0.178, 0.67, and 1.31 eV, respectively, above the $^2P_{3/2}$ ground states.[17]

Under the EI conditions described above, the spin–orbit composition of the Xe^+ and Kr^+ ion beams has been found to be near statistical, i.e., $(J=3/2):(J=1/2) \approx 2:1$.[18,19] Ion beams composed primarily of $Xe^+(^2P_{3/2})$ spin–orbit ground state ions are produced by using a high pressure flow tube source.[20] The addition of methane downstream from the ion source depletes the $Xe^+(^2P_{1/2})$ population and enhances the $Xe^+(^2P_{3/2})$ state, such that nearly 100% ground state $Xe^+(^2P_{3/2})$ beams are produced.[18] For verification, the low-energy reaction of the state-selected ion beam with methane is used as a diagnostic.[18] The charge–transfer reaction with $Xe^+(^2P_{3/2})$ ions is 0.47 eV endothermic, such that there is a distinct threshold in the cross section for this reaction, while reaction of the excited $Xe^+(^2P_{1/2})$ spin–orbit state is exothermic. The low-energy reaction of the beam with CH_4 is thus monitored while adjusting the pressure of methane in the flow tube. Based on this diagnostic, we are producing $Xe^+(^2P_{3/2})$ ion beams of $>99\%$ purity. The silane reactions are then measured without further changes in ion source conditions.

To produce ion beams of $Kr^+(^2P_{3/2})$ ions, carbon monoxide is introduced to the flow tube downstream from the ion source. Reaction of CO with Kr^+ ions has been shown to produce beams of primarily $Kr^+(^2P_{3/2})$.[19] Again, methane is used as a diagnostic since reaction of the $^2P_{3/2}$ state to form CH_3^+ is about 0.4 eV endothermic, such that this process is not allowed at low energies. The fraction of the spin–orbit states in the beam can be determined from the product ion intensities as described previously.[19] Based on the low-energy reactions of the Kr^+ ion beam with methane, we are producing $Kr^+(^2P_{3/2})$ ion beams of better than 95% purity.

Ion collection efficiency

For charge–transfer and dissociative charge–transfer reactions, products may be formed through a long-range electron jump such that little or no forward momentum is transferred to the ionic products.[21] In such instances, it is possible that up to 50% of these ions may have no forward velocity in the laboratory and will not drift out of the octopole to the detector. Such slow product ions which do traverse the octopole may be inefficiently transmitted through the quadrupole mass filter.[15] Exothermic or nearly thermoneutral reaction channels, in particular, can be subject to these effects. Nevertheless, results reported here were reproduced on several occasions and the cross section magnitudes shown are averaged results from all data sets. Based on reproducibility, the uncertainty in the absolute cross sections is estimated as $\pm 30\%$ in the Ne, Ar, Kr, and Xe systems. The uncertainty for the He systems is larger, 50%–60%, due to difficulties associated with collecting a low mass ion such as He^+, as discussed previously.[22] These uncertainties are conservative estimates, however, and our results will be found to agree nicely with previous experimental data.

Collision cross sections

The collision cross section σ_{col} for ion–molecule reactions at low energies is predicted by the Langevin–Gioumousis–Stevenson (LGS) model[23]

$$\sigma_{\text{LGS}} = \pi e (2\alpha/E)^{1/2}, \tag{1}$$

where e is the electron charge, α is the polarizability of the target molecule, and E is the relative kinetic energy of the reactants. Many exothermic reaction cross sections follow this type of energy dependence, although deviations are commonly seen.[24] The polarizability of SiH_4 is not well established, with literature values ranging from that of methane, 2.6, to 5.44 Å^3.[25] Haaland has recently measured $\alpha(SiH_4)$ and thoroughly reviewed the literature values. His recommended value for $\alpha(SiH_4)$ of 4.62 Å^3 is used here.[6]

At high kinetic energies, σ_{col} for charge–transfer reactions may best be represented by the hard-sphere limit, given by

$$\sigma_{\text{HS}} = \pi R^2. \tag{2}$$

R is roughly estimated as $r_e(Rg^+–H) + r_e(H_3Si–H)$, where $r_e(H_3Si–H) = 1.47$ Å.[6] For RgH^+, the r_e values used here are 1.59, 1.50, 1.28, 0.99, and 0.774 Å, for Rg = Xe, Kr, Ar, Ne, and He, respectively.[26] This results in $\sigma_{HS}(Xe^+–SiH_4) = 29$ Å^2, $\sigma_{HS}(Kr^+–SiH_4) = 28$ Å^2, $\sigma_{HS}(Ar^+–SiH_4) = 24$ Å^2, $\sigma_{HS}(Ne^+–SiH_4) = 19$ Å^2, and $\sigma_{HS}(He^+–SiH_4) = 16$ Å^2. In this work, σ_{col} is taken to be the maximum of σ_{LGS} and σ^{HS}.

Rate constants

In order to compare the present results with previous drift tube and ICR results, the cross sections must be converted into rate constants. The phenomenological rate constant is

$$k(\langle E\rangle) = v_0\sigma(E_{cm}), \tag{3}$$

where $v_0 = (2E_{cm}/\mu)^{1/2}$ and $\mu = mM/(m+M)$ is the reduced mass of the reactants. The rate constants are a function of the mean relative energy of the reactants, $\langle E\rangle = E_{cm} + (3/2)\gamma k_B T$, where $\gamma = m/(m+M)$ and T is the temperature of the reactant gas (300 K). In the limit that $E_{cm}\rightarrow 0$, $k(\langle E\rangle)$ approaches the "bulk" thermal rate constant for the temperature $T' = \gamma T$. In most cases, the room-temperature rate constant can be estimated by examining the behavior of $k(\langle E\rangle)$ at the lowest interaction energies. For the reactions studied here, estimates of $k(T=298\text{ K})$ are easily obtained because $k(\langle E\rangle)$ is essentially constant at low values of $\langle E\rangle$.

RESULTS

For the reaction of rare gas ions with SiH_4 there are four SiH_x^+ (x = 0–3) product ions observed in the energy ranges studied here, as given in reactions (4)–(7), where brackets indicate that the hydrogen can conceivably be liberated as either molecular hydrogen or separated atoms

$$Rg^+ + SiH_4 \rightarrow SiH_3^+ + Rg + H, \tag{4}$$

$$\rightarrow SiH_2^+ + Rg + [H + H], \tag{5}$$

$$\rightarrow SiH^+ + Rg + [H + H + H], \tag{6}$$

$$\rightarrow Si^+ + Rg + [H + H + H + H]. \tag{7}$$

Formation of SiH_4^+ and RgH^+ are not observed in any of the five rare gas systems. Formation of H^+ and H_2^+ were also observed by Chatham *et al.* for the reactions of Ar^+, Ne^+, and He^+ with silane.[7] Despite a careful search for these products, Haaland did not observe their formation in his ICR study, and attributes their presence in the drift tube experiments to impurity ionization.[6] Further, these species have not been observed in measurements of the electron impact ionization of silane.[27,28] This seems reasonable since the IEs of the silane radicals are all substantially lower than those of either atomic or molecular hydrogen, such that the likelihood of H^+ and H_2^+ formation is remote. For these reasons and because our present experimental configuration is not designed for good collection of these very light product ions, formation of H^+ and H_2^+ were not examined in the current study.

TABLE I. Thermochemical values at 298 K.[a]

Species (A)	$\Delta_f H(A)$ (kcal/mol)	$\Delta_f H(A^+)$ (kcal/mol)	IE(A) (eV)
Si	107.6±1.9	297.1±1.0	8.15±0.09
SiH	90.0±1.7	273.8±1.2	7.91±0.01
SiH_2	67.9±2.0	278.0±1.4	9.02±0.02
SiH_3	48.5±1.6	237.5±1.2	8.14±0.01
SiH_4	8.2±0.5	266.5±0.8	11.00±0.02[b]
H	52.10	367.17	13.598
He	0	568.48	24.587
Ne	0	498.80	21.565
Ar	0	364.91	15.760
Kr	0	324.32	14.000
Xe	0	281.20	12.130

[a]Unless otherwise noted, heats of formation for the silicon hydride species are the recommended values from Ref. 13. Values for H and the rare gases are taken from M. W. Chase, Jr., C. A. Davies, J. R. Downey, Jr., D. J. Frurip, R. A. McDonald, and A. N. Syverud, J. Phys. Chem. Ref. Data **14**, Suppl. 1, 1 (1985).
[b]Reference 41.

There are two complexities associated with analyzing the cross sections for the individual products of reactions (4)–(7) as a function of relative kinetic energy. First, since the Si atom exists as the ^{28}Si (92.23% natural abundance), ^{29}Si (4.67% natural abundance), and ^{30}Si (3.10% natural abundance) isotopes, the results obtained for a given mass can represent several product species. This is easily accounted for, and the absolute magnitudes of the cross sections shown here are results for single chemical species.[29] The second issue is the overlap of one mass with adjacent masses in the quadrupole mass filter used for product analysis. This can occur because mass resolution is sacrificed in order to transmit ions efficiently. In the present study, cross sections were measured with high mass resolution to determine the relative intensity of the products and with low mass resolution to verify efficient product collection.

Heats of formation given in Table I are used to calculate the reaction enthalpies for processes (4)–(7) for the five rare gas systems listed in Table II. We assume that the neutral reactants and the products formed at the threshold of an endothermic reaction are characterized by a temperature of 298 K in all degrees of freedom. Thus, we make no correction for the energy available in internal modes of the neutral reactant.

Helium

Figure 1 shows results for reactions (4)–(7) with Rg = He. The cross sections for all four reactions decrease with increasing energy, indicating that these products are formed in exothermic processes. This is consistent with the thermochemistry of Table II, which indicates that dissociative charge–transfer to form all four product ions is exothermic regardless of the neutral products. The total reaction of He^+ with silane is very efficient, proceeding at about 80% of the LGS collision limit at the lowest energies, and is nearly as large as σ_{col} at most other kinetic energies. Below ~2.0 eV, the cross sections all have a similar shape, and fall off as $E^{-0.40\pm0.03}$, slightly slower

TABLE II. Reaction thermochemistry at 298 K (eV).[a]

Process	Products	He	Ne	Ar	Kr	Xe
4	$SiH_3^+ + H + Rg$	−12.45	−9.43	−3.62	−1.86	0.003
5	$SiH_2^+ + 2H + Rg$	−8.43	−5.42	0.39	2.15	4.02
5	$SiH_2^+ + H_2 + Rg$	−12.95	−9.94	−4.12	−2.37	−0.50
6	$SiH^+ + 3H + Rg$	−6.36	−3.34	2.47	4.23	6.10
6	$SiH^+ + H + H_2 + Rg$	−10.87	−7.86	−2.05	−0.29	1.58
7	$Si^+ + 4H + Rg$	−3.09	−0.07	5.74	7.50	9.36
7	$Si^+ + 2H_2 + Rg$	−12.12	−9.11	−3.30	−1.54	0.33

[a]For the $J=3/2$ ground state of the Rg^+ ion (Rg = Ne, Ar, Kr, and Xe). The uncertainties are ±0.06 eV for reactions (4)–(6), and ±0.05 eV for reaction (7).

than the behavior predicted in Eq. (1). Formation of Si^+ and SiH^+, processes (6) and (7), dominate the observed reactivity at all energies in this system.

Neon

Results for the reaction of Ne^+ with SiH_4 are shown in Fig. 2. Similar to the He system, the cross sections for processes (5)–(7) are all observed to decrease with increasing energy, indicating exothermic processes. This is again consistent with the known thermochemistry of Table II, which indicates that dissociative charge–transfer to form all four product ions is exothermic regardless of the neutral products. In the Ne system, however, formation of SiH_3^+, process (4), is not observed at any energies. Thus the cross section magnitude for this process must be <0.01 Å^2. Below ~1.0 eV, the total cross section falls off as $E^{-0.62\pm0.04}$, slightly faster than the behavior predicted in Eq. (1). Above ~1.0 eV, the cross section levels off at about 10 Å^2, mimicking the behavior of σ_{col}. The reaction of Ne^+ with SiH_4 is much less efficient at all energies than the reaction of He^+, proceeding at only 35%–50% of σ_{col}, Fig. 2. Similar to the He system, however, the dominant reactions at all energies studied here are formation of SiH^+, process (6), and formation of Si^+, process (7).

Argon

Results for the reaction of Ar^+ with SiH_4 are shown in Fig. 3. Processes (4)–(7) are observed at all energies. In contrast to the He and Ne systems, reaction of Ar^+ with SiH_4 is extremely inefficient at low energies, proceeding at only ~3% σ_{LGS} at our lowest energies. The observed reactivity is primarily due to formation of SiH_3^+, process (4), which is favored over the other processes by nearly an order of magnitude. According to the thermochemistry of Table II, observation of all four product ions at thermal energies indicates that H_2 (rather than separated H atoms) must be one of the neutral products formed in reactions (5)–(7).

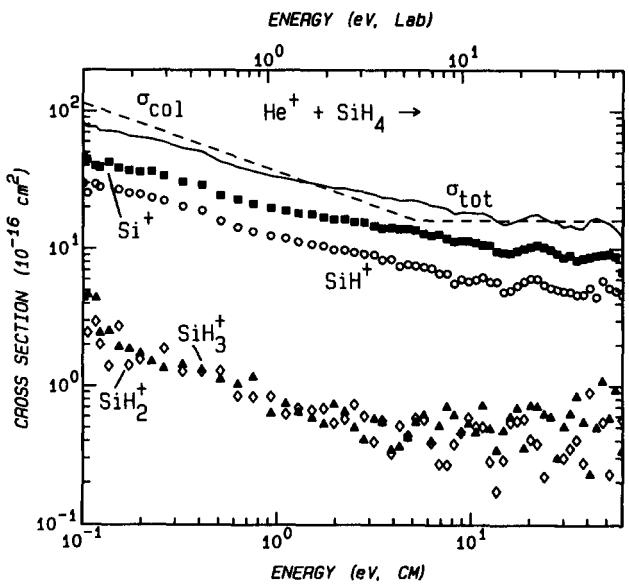

FIG. 1. The variation of product cross sections with translational energy in the laboratory frame of reference (upper scale) and the center-of-mass frame (lower scale) for the reaction of He^+ with SiH_4. The dashed line shows the collision cross section, given by the maximum of either the hard sphere or LGS [$\alpha(SiH_4) = 4.62$ Å^3] cross sections, Eqs. (1) and (2).

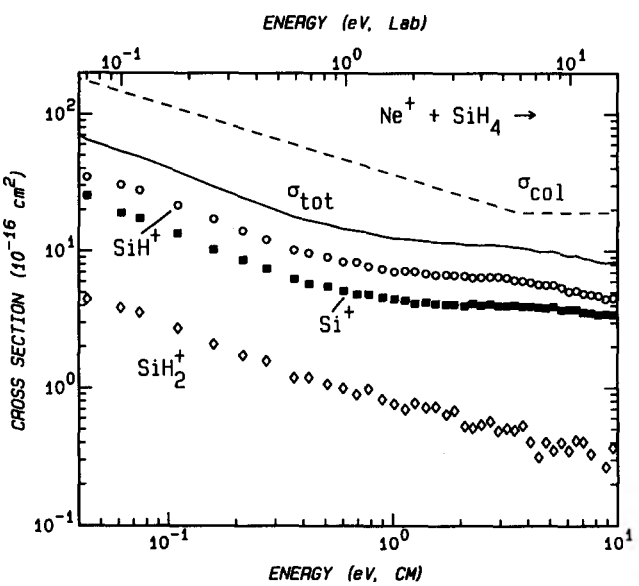

FIG. 2. The variation of product cross sections with translational energy in the laboratory frame of reference (upper scale) and the center-of-mass frame (lower scale) for the reaction of Ne^+ with SiH_4. The dashed line shows the collision cross section, given by the maximum of either the hard sphere or LGS [$\alpha(SiH_4) = 4.62$ Å^3] cross sections, Eqs. (1) and (2).

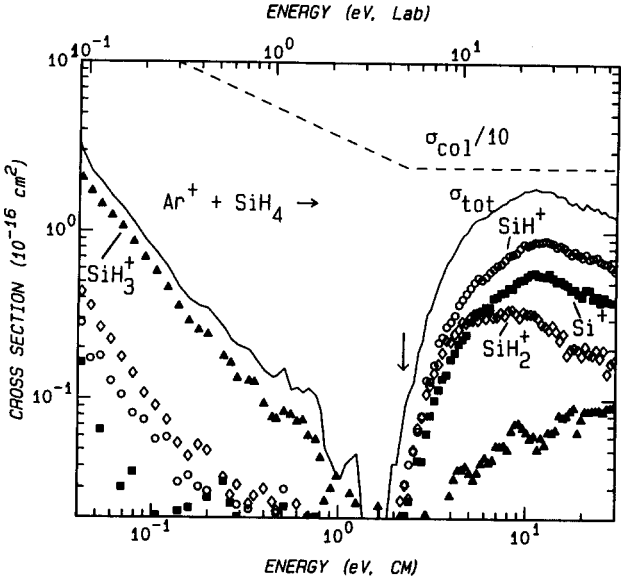

FIG. 3. The variation of product cross sections with translational energy in the laboratory frame of reference (upper scale) and the center-of-mass frame (lower scale) for the reaction of Ar^+ with SiH_4. The dashed line shows the collision cross section, given by the maximum of either the hard sphere or LGS [$\alpha(SiH_4) = 4.62$ Å^3] cross sections, Eqs. (1) and (2). The arrow indicates the ΔIE value for the $3a_1$ state of SiH_4 at 2.2 eV.

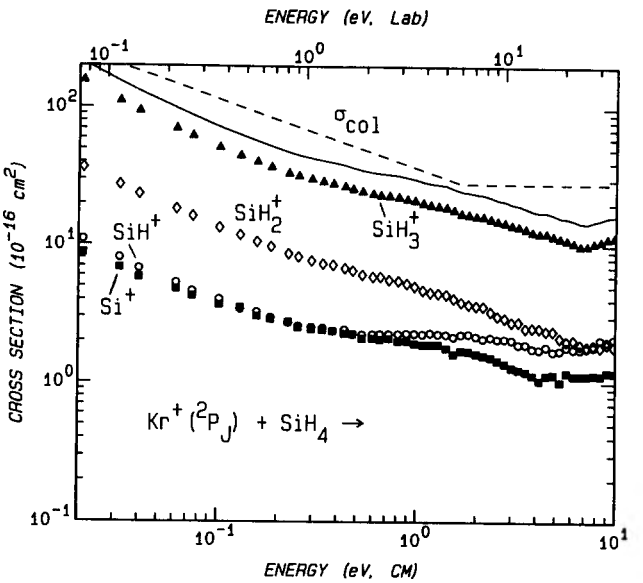

FIG. 4. The variation of product cross sections with translational energy in the laboratory frame of reference (upper scale) and the center-of-mass frame (lower scale) for the reaction of $Kr^+(^2P_J)$ with SiH_4. The solid line is the total cross section. The dashed line shows the collision cross section, given by the maximum of either the hard sphere or LGS [$\alpha(SiH_4) = 4.62$ Å^3] cross sections, Eqs. (1) and (2).

At our lowest kinetic energies, the total cross section for reaction of Ar^+ with silane falls off as $E^{-1.48\pm0.35}$, much faster than the predicted behavior of Eq. (1). As the kinetic energy increases, the product ion cross sections decrease until ~2.0 eV, where they increase dramatically, Fig. 3. At the highest kinetic energies, the maximum total cross section for the Ar systems reaches ~10% σ_{col}. At these high energies, the branching ratio is completely different from that at low energies and is dominated by Si^+ and SiH^+ formation.

Krypton

Results for reaction of Kr^+ produced by electron impact (having a statistical distribution of spin–orbit states) with SiH_4 are shown in Fig. 4. Processes (4)–(7) are observed, with the cross sections for all four product ions decreasing with increasing energies, indicating exothermic processes. Similar to the Ar system, this is consistent with the Table II thermochemistry if H_2 is formed as a neutral product in reactions (5)–(7). The reaction of Kr^+ with SiH_4 is much more efficient than that of Ar^+, proceeding at about 70% of the LGS collision limit at the lowest kinetic energies. Below ~0.8 eV, the cross sections all have a similar shape, and fall off as $\sim E^{-0.55\pm0.05}$, in good agreement with the behavior predicted in Eq. (1). The cross section for process (6) flattens out at energies >0.8 eV, remaining essentially constant out to the highest energies. Similar to the low energy results in the Ar system, the dominant process at all energies in the Kr system is formation of SiH_3^+.

State-specific results for the reaction of $Kr^+(^2P_{3/2})$ with silane are very similar to the results of Fig. 4, with formation of SiH_3^+ dominating the reactivity at all energies. For $Kr^+(^2P_{3/2})$, however, ~20% more Si^+ than SiH^+ is formed at low kinetic energies, whereas in the EI data, SiH^+ dominates over Si^+ at these energies by ~10%.

Xenon

Results for reaction of Xe^+ (with a statistical distribution of spin–orbit states) with SiH_4 are shown in Fig. 5. The total reaction for Xe^+ with silane is very efficient, proceeding at essentially the LGS collision limit at the lowest energies. The only reactions observed in the energy range studied here are formation of SiH_3^+, process (4) and formation of SiH_2^+, process (5). This indicates that the cross section magnitudes for processes (6) and (7) must be <0.01 Å^2. The reaction cross sections for both processes observed decrease with increasing energies, indicating exothermic reactions. This is consistent with the thermochemistry of Table II if H_2 is formed in reaction (5), and by noting that reaction (4) is thermoneutral for $Xe^+(^2P_{3/2})$ and exothermic for $Xe^+(^2P_{1/2})$.

Below ~0.3 eV, the cross section for process (5) decreases as $\sim E^{-0.25\pm0.05}$, significantly slower than the behavior predicted by Eq. (1). The cross section for process (4) has a slightly different energy dependence, decreasing as $\sim E^{-0.45\pm0.05}$ below 0.3 eV, in good agreement with the behavior predicted by Eq. (1). At energies greater than ~0.2 eV, the cross section for reaction (4) levels off and is essentially constant out to the highest energies. These different energy dependencies mean that formation of SiH_2^+, process (5), is favored over process (4) below ~0.5 eV, but SiH_3^+ formation is favored above ~0.5 eV. This probably results because formation of SiH_3^+ is less

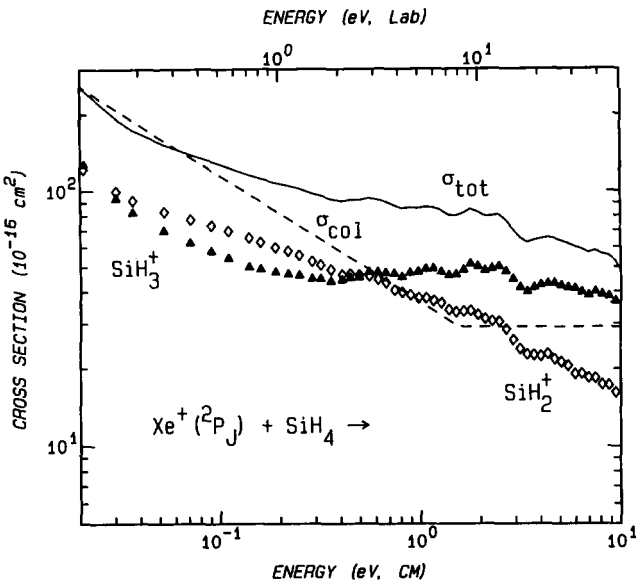

FIG. 5. The variation of product cross sections with translational energy in the laboratory frame of reference (upper scale) and the center-of-mass frame (lower scale) for the reaction of Xe^+ (^2P_J) with SiH_4. The dashed line shows the collision cross section, given by the maximum of either the hard sphere or LGS [$\alpha(SiH_4) = 4.62$ Å^3] cross sections, Eqs. (1) and (2).

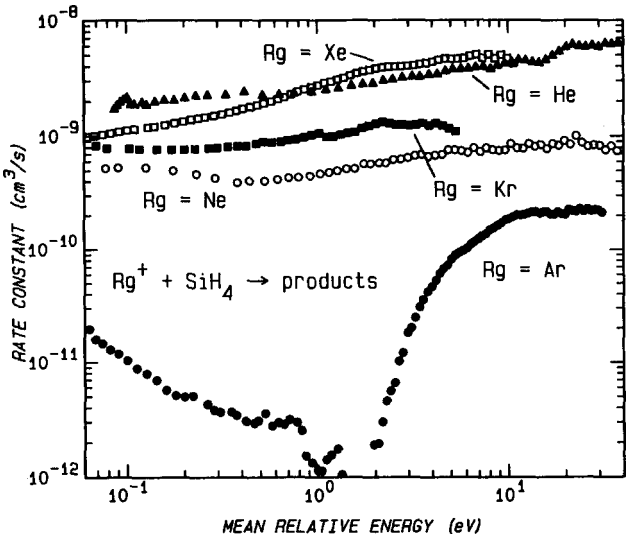

FIG. 6. Phenomenological rate constants for the reaction Rg^+ + SiH_4 (Rg = He, Ne, Ar, Kr, and Xe) as a function of mean relative energy. These are derived from the data of Figs. 1–5 by using Eq. (3).

exothermic than formation of SiH_2^+, but kinetically favored (since H_2 elimination should have a tight transition state, while H atom loss does not).

The state-specific results for the reaction of Xe^+ ($^2P_{3/2}$) with silane lead to cross sections for processes (4) and (5) that are very similar to those of Fig. 5. The main difference between the EI data of Fig. 5, and the ground state data is in the absolute magnitudes of the cross sections. For Xe^+ ($^2P_{3/2}$), the magnitude for the SiH_2^+ cross section increases by ~20% throughout the energy region examined. The SiH_3^+ cross section remains the same below 0.2 eV, but increases by 20% above this energy. Process (4) again dominates the observed reactivity above ~0.6 eV.

DISCUSSION

Reaction rates

Although thermal energy rates for many reactions occurring in a plasma environment have been measured or estimated, the collection of kinetic data for these systems is not complete since reaction rates over a wide range of energies are rarely available. Figure 6 shows our cross sections converted with Eq. (3) to total reaction rate constants as a function of energy for all five reaction systems. The rate constants for Rg = He, Ne, and Kr are relatively constant at all energies. The Ar system is markedly different from the other rare gas systems. The reaction rate *decreases* steadily from the lowest energies to ~2 eV, where it rises sharply to reach a maximum of $\sim 2\times10^{-10}$ cm^3 s^{-1}.

Thermal reaction rate constants for the exothermic reactions measured here are given in Table III along with other literature values and the LGS rate constants. Reactions of the five rare gas ions with SiH_4 were first studied by Bowers and Elleman (BE) using ICR techniques.[5] Total rates for these reactions were reported without observation of the individual silicon hydride ion products. They found that the total charge exchange rates for most of the rare gas ions were very fast, proceeding at >75% of the collision rate. The exception was the reaction of Ar^+ which proceeds at ~10% of the collision rate according to BE. Chatham, Hils, Robertson, and Gallagher (CHRG)[7] examined the reactions of He^+, Ne^+, and Ar^+ ions with silane in a drift tube: quadrupole mass spectrometer apparatus, and reported rate constants as a function of energy over the energy range 0.1–1.0 eV. The thermal rate coefficients given by CHRG are given in Table III. They report a total reaction rate for the Ar system that is only 2% of the collision rate, <20% of BE's value. In addition to these two studies, thermal rate constants for each of the noble gas–silane systems were measured recently by Haaland using ICR experiments, Table III.[6] The thermal reaction rates reported in this study for He^+, Ne^+, Ar^+, and Xe^+ were at least 20% lower than those of BE, while that for Kr^+ was ~40% higher than BE's value.

The total reaction rate for charge–transfer of He^+ with silane reported here is in very good agreement with two of the previous three studies, Table III, and within the combined experimental uncertainties of the ICR study of Haaland. The rate constants from the three previous studies of the Ne reaction are in reasonable agreement, while our results are smaller, but within the combined experimental errors. In the Ar^+ + SiH_4 system, we measure a total rate for reaction that is 1 order of magnitude lower than that found for the Ne system, and nearly 2 orders of magnitude smaller than the rate for the He system, Table III. Our value is twice that of CHRG and about half those of Haaland and BE, but is within experimental error of the

TABLE III. Thermal reaction rate constants.[a]

Rg ion	Present[b]	Haaland[c]	CHRG[d]	BE[e]	LGS[f]
He^+	23.5(9.0)	16.0(2.0)	24.0(5.0)	21.8(4.0)	26.7
Ne^+	5.3(1.6)	6.7(2.0)	8.5(1.7)	8.5(1.7)	14.3
Ar^+	0.39(0.11)	0.8(0.3)	0.17(0.1)	1.0(0.2)	11.9
$Kr^+(^2P_{3/2})$	7.7(1.5)	12.0(3.5)[g]		8.5(1.7)[g]	10.4
$Kr^+(^2P_{1/2})$	6.0(1.8)				10.4
$Xe^+(^2P_{3/2})$	9.4(1.9)	5.1(1.0)[g]		8.4(1.7)[g]	9.9
$Xe^+(^2P_{1/2})$	7.0(2.1)				9.9

[a]All rates in units of 10^{-10} cm^3 s^{-1}. Uncertainties in parentheses.
[b]Present results.
[c]ICR studies of Haaland, Ref. 6.
[d]Drift tube: quadrupole mass spectrometry studies of CHRG, Ref. 7. Results are for a temperature of 700 K. Assumed 20% error.
[e]ICR studies of BE, Ref. 5. Assumed 20% error.
[f]Langevin–Gioumousis–Stevenson collision rate, Eq. (1) with $\alpha(SiH_4) = 4.62$ Å^3.
[g]Values are for an unspecified distribution of spin–orbit states.

results of Haaland and CHRG. For the Kr and Xe systems, we obtain reaction rates for both spin–orbit states and these are listed in Table III. [Values for $Kr^+(^2P_{1/2})$ and $Xe^+(^2P_{1/2})$ are derived by extrapolation from the EI and $^2P_{3/2}$ cross section data.][30] Our results indicate that reaction of the ground states are very efficient, proceeding at about 75% and 95% of the Langevin rate, respectively; both excited states are less reactive by about 25%. These two rare gases were not studied by CHRG, but our results are in reasonably good agreement with the previous work of BE given that the spin–orbit state distribution is unknown.

While the agreement between the various rate constant measurements is satisfactory, several experimental considerations may explain the origins of the discrepancies that are observed. First, as discussed in the Experimental section, it is possible that ion collection in our experiment is inefficient for charge–transfer reactions, especially those involving low mass ions such as He^+. The good agreement between the present results and LGS predictions as well as previously measured rate constants for the He, Kr, and Xe systems indicate that this is not a likely source of error in the systems studied here. While the rate constant for the Ne system is somewhat lower than previously measured, it seems improbable that ion collection efficiency would be worse for this system than for the He system. Second, the ion source conditions in the various experiments differ. BE do not explicitly state how their rare gas ions are produced, but typical ICR source conditions use electron impact ionization at electron energies $\geqslant$50 eV. In Haaland's ICR experiments, most of the data was collected at electron energies $<$50 eV,[6] while in the drift tube experiments of CHRG, electron energies of either 50 or 100 eV were used.[7] Thus, some of the observed variations in rate constants for the rare gas/silane systems may be due to differences in the amount of highly excited ions present in the ICR and drift tube experiments. This problem is avoided in the present results by controlling the electron energy used to form the ions such that electronic distribution of the ions is characterized, as described above. Third, in the drift tube experiments, CHRG note that their ions may be undergoing secondary collisions, which could alter the observed reaction rates and change the product branching ratios.[7] This is not a consideration in the present or ICR experiments.

A fourth consideration peculiar to the case of Ar^+ is the strong kinetic energy dependence for this reaction, Fig. 6. Clearly, small variations in the system temperature can make a large difference in the measured rate constant for this system. For example, the low value of the rate constant cited by CHRG is actually for a temperature of 700 K ($\frac{3}{2}kT = 0.09$ eV). At this energy, we measure a rate constant of 0.13×10^{-10} cm^3 s^{-1}, Fig. 6, in excellent agreement with CHRG. Differences between our thermal (300 K) rate constant and those of the ICR experiments may indicate that the ion energy distribution is colder in these experiments than in the beam work. As discussed previously,[31] our ion beams have an energy distribution at the lowest kinetic energies that is skewed to slightly higher energies and is wider than a Maxwell–Boltzmann (MB) distribution. Distributions in ICR experiments are poorly characterized but are probably close to a MB distribution.

Branching ratios

The observed product branching ratios in both the He and Ne systems are virtually energy independent. For the He system, the product distribution for processes (4)–(7) is 3:4:38:56. This is in agreement with the results of Chatham, Hils, Robertson, and Gallagher (CHRG),[7] who found that the rate constant and branching ratio was energy independent between 0.1 and 1 eV, with relative intensities of $SiH_2^+ < SiH^+ \approx H^+ < Si^+$. CHRG do not observe formation of SiH_3^+. Based on CHRG's figure of rate constants as a function of energy (Fig. 9, Ref. 7), a rough estimate of the branching ratio, SiH_2^+:SiH^+:Si^+, yields 1:37:62. This is roughly the same partitioning between the major products SiH^+ and Si^+ observed here. A similar

TABLE IV. Adiabatic and vertical ionization energies for SiH_4 [a].

Orbital	Adiab.	Vert.	ΔIE(He)[b]	ΔIE(Ne)[b]	ΔIE(Ar)[b]	ΔIE(Kr)[b]	ΔIE(Xe)[b]
$2t_2$	11.6	12.82	−12.37	−9.35	−3.54	−1.79	0.08
$3a_1$	17.95	18.17	−6.52	−3.50	2.30	4.06	5.93
		24.2[c]	−0.38	2.64	8.44	10.20	12.07

[a]Except where noted, values are taken from Ref. 32.
[b]ΔIE(Rg) = IE(orbital) − IE(Rg), where IE(orbital) is the mean of the adiabatic and vertical values and IE(Rg) is for the ground state of the rare gas ion taken from Table I.
[c]Values from Ref. 36.

partitioning of 33:67 is observed by Haaland who does not observe the production of SiH_3^+, H^+, or H_2^+ in the He system.[6]

In the Ne system, we obtain a product branching ratio for formation of SiH_2^+, SiH^+, and Si^+ [processes (5), (6), and (7)] of 8:54:37. SiH_3^+ accounts for $<1\%$ of the products in this system. This is also in qualitative agreement with the low energy results of CHRG, who found relative intensities of $SiH_2^+ \ll Si^+ < H^+ < SiH^+$, and no production of SiH_3^+. Again, a rough estimate of the branching ratio from CHRG's figure of rate constants as a function of energy (Fig. 9, Ref. 7) yields 10:60:30 at 0.1 eV for SiH_2^+:SiH^+:Si^+. At higher energies, CHRG's results show a reverse in the partitioning between SiH^+ and Si^+, giving an approximate branching ratio of 4:29:67 at 1.0 eV. This switch at higher kinetic energies is not observed here and could be the result of secondary collisions in the drift tube studies. The results of Haaland are also in agreement with the present results and the low energy results of CHRG, with SiH^+ formation dominating over Si^+ formation.[6] In addition, Haaland does not observe the production of SiH_3^+, H^+, or H_2^+ in the Ne system.

In the Ar system at low energies, the product distribution for processes (4)–(7) is 78:12:8:2 and is independent of kinetic energy below 2.0 eV. Above 2 eV, the branching ratio almost completely reverses and reaches 4:16:50:30 at energies $\geqslant 10$ eV. Thus, at high kinetic energies, formation of the smaller product ions, processes (6) and (7), are favored much more than reactions (5) and (4), a result similar to the He and Ne systems.

The thermal energy product distribution results of CHRG for the reaction of Ar^+ with silane do not agree with those determined here. CHRG find that the low energy (0.1 eV) branching ratio between processes (4)–(7) is 12:21:8:59, i.e., $SiH^+ < SiH_3^+ < SiH_2^+ < Si^+$. However, the results of Haaland for the same reaction at thermal energy show exclusive formation of SiH_3^+,[6] in good agreement with the results found here at the lowest kinetic energies. The disagreement with the results of CHRG is possibly explained by noting that CHRG estimate that at the collision energies used (0.1–1.0 eV), as many as 25% of the product ions could have undergone secondary, hydrogen-stripping reactions. In contrast, the results presented here are obtained under conditions such that secondary collisions are improbable.

At the lowest energies, the product branching ratio between processes (4)–(7) in the $Kr^+(^2P_J)$ system is 70:19:6:5. For the $Kr^+(^2P_{3/2})$ system, the branching ratio between processes (4)–(7) at these energies is 75:17:3:5. Using the EI and $^2P_{3/2}$ data, we can extrapolate to $^2P_{1/2}$ cross sections and determine a $Kr^+(^2P_{1/2})$ branching ratio of 55:26:12:7.[30] The branching ratio for the Kr system is very similar to the low energy results in the Ar system, and contrast with the results of the He and Ne systems. The only product observed in the ICR experiments of Haaland is SiH_3^+.

The product distribution between processes (4) and (5) in the $Xe^+(^2P_J)$ system is 48:52 at the lowest energies. Above ~0.4 eV, formation of SiH_3^+ becomes the favored process, and the branching ratio increases to 69:31 by 10.0 eV. The product distribution at low energies between processes (4) and (5) for the $Xe^+(^2P_{3/2})$ ground spin–orbit state has changed only slightly from the EI results, 44:56. Again the branching ratio shifts at energies above ~10 eV to 74:26, similar to the EI results. At intermediate energies (0.04–0.2 eV), the branching ratio is ~40:60 for both systems. Similar to the Kr system, we can use both sets of data to extrapolate to $^2P_{1/2}$ cross sections[30] and derive a $Xe^+(^2P_{1/2})$ low energy branching ratio identical to the $^2P_{3/2}$ results, and a high energy branching ratio ($\geqslant 10$ eV) of 50:50. Our low energy results are in agreement with the thermal energy results of Haaland who found that only SiH_3^+ and SiH_2^+ are formed, with a partitioning of approximately 37:63.

General behavior and relative reactivity

The product branching ratios and the unique behavior displayed in the product cross sections of the Ar system can be understood by examining the photoelectron spectrum (PES) of SiH_4.[32–34] Other measurements for the ionization energies of SiH_4 are available from x-ray PES[35] and electron momentum spectroscopy (EMS).[36] Table IV lists the vertical and adiabatic ionization energies for SiH_4 from the PES of Potts and Price,[32] and from the EMS of Clark *et al.*[36] Further bands at higher binding energy have been detected by EMS, Table IV. The difference between SiH_4 ionization energies and the ionization potentials of the rare gases, ΔIE, are also listed in Table IV.

It is interesting to note that the two different bands in the PES of SiH_4 result from removal of an electron from very different molecular orbitals (MOs). While both the $2t_2$ and $3a_1$ orbitals on silane are bonding, the $3a_1$ MO is produced from the Si(3*s*) and H(1*s*) atomic orbitals, and

is thus totally symmetric, while the $2t_2$ MOs are constructed from the Si($3p$) and H($1s$) atomic orbitals and have a planar node.[35] Ionization and subsequent dissociation of SiH_4 by removal of an electron from these two orbitals might therefore be expected to proceed by different mechanisms. Indeed, this is observed in the results of Cooper, Ibuki, and Brion (CIB) who studied the photoionization, photoabsorption, and ionic photofragmentation of both the valence shell[37] and the inner shell[38] of silane. CIB found that for photons having energies less than 17.95 eV (the IE of the $3a_1$ orbital of silane), SiH_3^+ and SiH_2^+ were the dominant fragment ions formed, with only small amounts of SiH^+ and Si^+. Above the $3a_1$ threshold, however, they found considerably larger amounts of the smaller fragment ions, with no increase in the production of the larger fragment ions. This leads to the conclusion that ionization from the $3a_1$ orbital proceeds exclusively to formation of SiH^+ and Si^+, whereas ionization from the $2t_2$ orbitals leads preferentially to formation of SiH_2^+ and SiH_3^+.

Theoretical results of Haaland also support this conclusion.[6] *Ab initio* electronic calculations for the silicon hydride cations show that loss of a $2t_2$ electron from silane leads to substantial reorganization of the molecule's electronic structure.[6] The molecular cation then adiabatically dissociates into $SiH_3^+ + H$ or $SiH_2^+ + H_2$. Conversely, the molecular cation formed by removal of a $3a_1$ electron is not subject to the same Jahn–Teller distortions, such that the influence of this electron loss affects the Si–H bonding symmetrically, changing all four bonds equally. This suggests that removal of a $3a_1$ electron will lead to the more dissociated product ions, SiH^+ and Si^+. Haaland uses this to explain his thermal energy results for the reactions of rare gas ions with silane, and concludes that given the IEs of a reactant ion, products as well as general reaction efficiencies can be predicted.[6]

These ideas help explain the efficiency of charge–transer and the differences in product branching ratios found here for the $Rg^+ + SiH_4$ systems, as well as the energy dependence of the branching ratio in the Ar system. In the Xe system, the Xe^+ ions are nearly resonant with the $^2T_2$ band in the SiH_4^+ PES ($\Delta IE = 0.08 \pm 0.21$ eV). Thus, the reaction efficiency is high at all energies and only formation of SiH_3^+ and SiH_2^+ is seen. Kr^+ is not nearly as resonant with the $^2T_2$ state of SiH_4^+, and hence the reaction efficiency declines. Again, the reaction system must access the $^2T_2$ band of the PES, since the SiH_x^+ product branching ratio heavily favors the SiH_3^+ and SiH_2^+ products. For the He and Ne systems, reaction is fairly efficient, and the branching ratios favor the smaller fragment ions SiH^+ and Si^+. This is consistent with near resonant charge–transfer from He^+ or Ne^+ to the broad band of the $^2A_1$ state of SiH_4^+, Table IV.

The Ar system offers an interesting intermediate case. Argon ions are not resonant with either the $^2T_2$ or the $^2A_1$ states of SiH_4^+, and only the $^2T_2$ state is energetically accessible at low kinetic energies. Thus, the charge–transfer reaction is very inefficient and the product branching ratio is characteristic of the $^2T_2$ state. As the kinetic energy is increased, the charge–transfer reaction falls further out of resonance until the formation of the $^2A_1$ state becomes accessible at 2.2 eV, the difference between IE(Ar) and the adiabatic IE for this state. This energy agrees nicely with the sharp onset for the second features in the SiH_x^+ ($x = 0$–3) cross sections, Fig. 3. Further, above this energy, the experimental branching ratio switches to that characteristic of the $^2A_1$ band. Thus, the distinctive cross section shape and the variation in product distributions in the $Ar^+ + SiH_4$ dissociative charge–transfer reaction are governed directly by the ability of the reaction system to access different electronic states of the SiH_4^+ ion. Similar coupling between kinetic and electronic energy has been seen previously in the reactions of rare gas ions with CF_4.[8]

In all five rare gas systems, formation of SiH_4^+ is not seen. This observation is consistent with results of electron impact studies which indicate that SiH_4^+ is not stable under collisionless conditions on a millisecond time scale.[6] Results of Hayaishi *et al.* indicate that the lifetime of the parent SiH_4^+ ion is less than a few tenths of μs.[39] Although the molecular cation has been observed in the photoionization spectrum of SiH_4, it is only observed over a very narrow energy range (between 11 and 12 eV).[40,41] In addition, the SiH_4^+ ion is nonlinear and orbitally degenerate, so it is highly subject to Jahn–Teller distortions from T_d symmetry. Based on *ab initio* calculations, the T_d molecular ion formed by vertical excitation of the molecule is expected to adiabatically dissociate to $SiH_3^+ + H$.[42]

Relation to plasma systems

To predict the optimum physical parameters of a plasma system, it is first necessary to understand the interactions at the substrate and ascertain the primary chemical species responsible for the desired deposition or etching process. The gas-phase chemistry can then be tailored by modifying the starting materials and bias of the substrate to obtain the maximum concentration of reactive species.

Although the role of ions in plasma deposition processes is not certain, silicon hydride ions have been observed in silane plasma systems[43–45] and have been suggested as important reactive species in deposition processes.[14,43,46] Specifically, silane is used extensively in plasma systems for the deposition of amorphous silicon. It has been proposed by Haaland[6] and others[4,14] that monosilicon hydride ions SiH_x^+ are responsible for thin film deposition in these systems. If true, then the optimum buffer gases to use would be those which produce the most SiH_3^+ and SiH_2^+, since the smaller silicon hydride ions have been shown to readily cluster into unsaturated disilicon hydride cations.[6] The present results suggest the use of krypton or xenon as bath gases over helium or neon. Argon might also be of use, but only if the bias energy is kept to a minimum, since at high kinetic energies the branching ratio favors the formation of the smaller silicon hydride ions. Another consideration, however, is the overall rate of silicon hydride ion formation, which should be fast. This would suggest the use of krypton or xenon over argon since

the argon reaction is extremely inefficient at all energies, reaching a maximum efficiency of only $\sim 10\%$ σ_{col}.

ACKNOWLEDGMENT

This work was funded by the Air Force Wright Aeronautical Laboratories.

[1] J. W. Coburn and H. F. Winters, J. Appl. Phys. **50**, 3189 (1979).
[2] *Amorphous Semiconductors*, edited by M. H. Brodsky (Springer, Berlin, 1979); I. Shimizu, T. Komatsu, K. Saito, and E. Inoue, J. Non-Cryst. Solids **35**, 773 (1980).
[3] D. E. Carlson, C. W. Magee, and A. R. Triano, J. Electrochem. Soc. **126**, 688 (1979).
[4] J. C. Knights, R. A. Lujan, M. P. Rosenblum, R. A. Street, D. K. Bieglesen, and J. A. Reimer, Appl. Phys. Lett. **38**, 331 (1981).
[5] M. T. Bowers and D. Elleman, Chem. Phys. Lett. **16**, 486 (1972).
[6] P. Haaland, Tech. Rep. AFWAL-TR-88-2043, Aero Propulsion Lab., Air Force Wright Aeronautical Lab., Wright–Patterson Air Force Base, Ohio, 1988.
[7] H. Chatham, D. Hils, R. Robertson, and A. C. Gallagher, J. Chem. Phys. **79**, 1301 (1983).
[8] E. R. Fisher, M. E. Weber, and P. B. Armentrout, J. Chem. Phys. **92**, 2296 (1990).
[9] M. E. Weber and P. B. Armentrout, J. Chem. Phys. **88**, 6898 (1988).
[10] M. E. Weber and P. B. Armentrout, J. Chem. Phys. **90**, 2213 (1989).
[11] M. E. Weber and P. B. Armentrout, J. Phys. Chem. **93**, 1596 (1989).
[12] B. H. Boo and P. B. Armentrout, J. Phys. Chem. **91**, 5777 (1987); B. H. Boo, J. L. Elkind, and P. B. Armentrout, J. Am. Chem. Soc. **112**, 2083 (1990).
[13] B. H. Boo and P. B. Armentrout, J. Am. Chem. Soc. **109**, 3549 (1987).
[14] H. Chatham and A. Gallagher, J. Appl. Phys. **58**, 159 (1985).
[15] K. M. Ervin and P. B. Armentrout, J. Chem. Phys. **84**, 6738 (1986).
[16] E. Teloy and D. Gerlich, Chem. Phys. **4**, 417 (1974).
[17] C. E. Moore, Natl. Stand. Ref. Data Ser. [Natl. Bur. Stand. (U.S.)] **34**, (1970).
[18] K. M. Ervin and P. B. Armentrout, J. Chem. Phys. **90**, 118 (1989).
[19] K. M. Ervin and P. B. Armentrout, J. Chem. Phys. **85**, 6380 (1986).
[20] R. S. Schultz and P. B. Armentrout, Int. J. Mass Spectrom. Ion Process. (submitted).
[21] P. M. Hierl, V. Pacak, and Z. Herman, J. Chem. Phys. **67**, 2678 (1977).
[22] K. E. Ervin and P. B. Armentrout, J. Chem. Phys. **86**, 6240 (1987).
[23] G. Gioumousis and D. P. Stevenson, J. Chem. Phys. **29**, 292 (1958).
[24] P. B. Armentrout, in *Structure/Reactivity and Thermochemistry of Ions*, edited by P. Ausloos and S. G. Lias (Reidel, Dordrecht, 1987), pp. 97–164.
[25] A. Maryott and F. Buckley, Natl. Bur. Stand. (U.S.) Circular 537, 1953.
[26] K. P. Huber and G. Herzberg, *Molecular Spectra and Molecular Structure: Constants of Diatomic Molecules* (Van Nostrand Reinhold, New York, 1979).
[27] F. Saalfeld and H. Svec, Inorganic Chemistry **2**, 46 (1963).
[28] G. Turban, Y. Catherine, and B. Grolleau, Thin Solid Films, **67**, 309 (1980).
[29] Since the signal at mass 29 is due to $^{28}SiH^+$ and $^{29}Si^+$, the cross section for mass 28 (which is due entirely to the $^{28}Si^+$ product) is scaled by the ^{28}Si:^{29}Si isotope ratio, 0.051, and subtracted from the mass 29 cross section. A similar procedure can then be followed for the mass 30 (due to $^{28}SiH_2^+$, $^{29}SiH^+$, and $^{30}Si^+$) and mass 31 (due to $^{28}SiH_3^+$, SiH_2^+, and $^{30}SiH^+$) cross sections. This process yields results for the $^{28}SiH_x^+$ product ions. The cross section for mass 33 is due entirely to $^{30}SiH_3^+$, and is used for verification of the magnitude of the $^{28}SiH_3^+$ cross section. After the $^{28}SiH_x^+$ product cross sections are determined, they are scaled by 1.084 (accounting for the natural abundance of ^{28}Si) to yield the results presented here as a single chemical species.
[30] The $^2P_{1/2}$ excited spin–orbit state cross sections are derived by scaling the $^2P_{3/2}$ data by 0.667, subtracting the result from the EI data, and then multiplying by a factor of 3 to arrive at the true state-specific behavior of the cross sections.
[31] J. D. Burley, K. M. Ervin, and P. B. Armentrout, J. Chem. Phys. **86**, 1944 (1987).
[32] A. W. Potts and W. C. Price, Proc. R. Soc. London Ser. A **326**, 165 (1972).
[33] B. P. Pullen, T. A. Carlson, W. E. Moddeman, G. K. Schweitzer, W. E. Bull, and F. A. Grimm, J. Chem. Phys. **53**, 768 (1970).
[34] G. G. B. de Souza, P. Morin, and I. Nenner, Phys. Rev. A **34**, 4770 (1986); T. Heinis, K. Börlin, and M. Jungen, Chem. Phys. Lett. **110**, 429 (1984).
[35] W. B. Perry and W. L. Jolly, J. Electron Spectrosc. Rel. Phenom. **4**, 219 (1974).
[36] S. A. C. Clark, E. Weigold, C. E. Brion, E. R. Davidson, R. F. Frey, C. M. Boyle, W. von Niessen, and J. Schirmer, Chem. Phys. **134**, 229 (1989).
[37] G. Cooper, T. Ibuki, and C. E. Brion, Chem. Phys. **140**, 133 (1990).
[38] G. Cooper, T. Ibuki, and C. E. Brion, Chem. Phys. **140**, 147 (1990).
[39] T. Hayaishi, T. Koizumi, T. Matsuo, T. Nagata, Y. Sato, H. Shibata, and A. Yagishita, Chem. Phys. **116**, 151 (1987).
[40] W. Genuit, A. Boerboom and T. Govers, Int. J. Mass Spectrom. Ion Process. **62**, 1770 (1984).
[41] J. Berkowitz, J. P. Greene, H. Cho, and B. Ruscic, J. Chem. Phys. **86**, 1235 (1987).
[42] M. Gordon, Chem. Phys. Lett. **59**, 410 (1978).
[43] I. Haller, Appl. Phys. Lett. **37**, 282 (1980); I. Haller, IBM Research Report, RC 14863 (#66580), Chemistry, IBM Research Division, T. J. Watson Research Center, Yorktown Heights, New York 10598.
[44] J. W. Coburn, H. F. Winters, and T. J. Chuang, J. Appl. Phys. **48**, 3532 (1977).
[45] G. Turban, Y. Catherine, and B. Grolleau, Plasma Chem. Plasma Proc. **2**, 61 (1982).
[46] C. A. DeJoseph, Jr., P. D. Haaland, and A. Garscadden, IEEE Trans. Plasma Sci. **PS-14**, 165 (1986).